

TESTING THE ORIGIN OF HIGH-ENERGY COSMIC RAYS

A. E. VLADIMIROV¹, G. JÓHANNESSON³, I. V. MOSKALENKO^{1,2}, AND T. A. PORTER¹

Submitted to The Astrophysical Journal

ABSTRACT

Recent accurate measurements of cosmic-ray (CR) protons and nuclei by ATIC-2, CREAM, and PAMELA reveal: a) unexpected spectral hardening in the spectra of CR species above a few hundred GeV per nucleon, b) a harder spectrum of He compared to protons, and c) softening of the CR spectra just below the break energy. These newly-discovered features may offer a clue to the origin of the observed high-energy Galactic CRs. We discuss possible interpretations of these spectral features and make predictions for the CR isotopic ratios, anisotropy of CRs, and diffuse Galactic γ -ray emission in different phenomenological scenarios. Our predictions can be tested by currently running or near-future high-energy astrophysics experiments.

Subject headings: astroparticle physics — diffusion — elementary particles — cosmic rays — ISM: general — dark matter — diffuse radiation — gamma rays: ISM — infrared: ISM — radio continuum: ISM — X-rays: ISM

1. INTRODUCTION

The spectrum of CRs has offered few clues to its origin so far. The only features observed are at very-high and ultra-high energies (see, e.g., Figure 1 in Swordy 2001): the so-called “knee” at a few times 10^{15} eV (Kulikov & Khristiansen 1958; Haungs et al. 2003), the second “knee” at $\sim 10^{18}$ eV, the “ankle” at higher energies (Abbasi et al. 2005), and a spectral steepening above 10^{20} eV (Abbasi et al. 2009; Abraham et al. 2010). Because of the limited size of Galactic accelerators and strength of magnetic fields in the acceleration region (e.g., in supernova remnants [SNRs]), it is believed that the CRs below the knee are Galactic, while above the knee they have an extragalactic origin, with the knee itself being due to propagation effects and a transition between the two populations of CRs (Berezinskii et al. 1990; Strong et al. 2007).

The power-law spectrum below the knee is thought to be the result of CR acceleration in SNR shocks (see, e.g., Drury et al. 2001), which is steepened by propagation in the interstellar medium (ISM) and eventual leakage from the Galaxy to the observed index ~ 2.75 . The interstellar diffusion coefficient is typically assumed to be a power-law in particle rigidity, based on numerous studies of magnetohydrodynamical turbulence (see, e.g., Biskamp 2003). The turbulent cascade often leads to a distribution of magnetic energy that is well described by a power law. For energies below ~ 20 GeV per nucleon, the CR spectrum flattens due to the modulation in the heliosphere – a combined effect of the solar wind and heliospheric magnetic field. Measurements of CR composition below a few GeV per nucleon offer detailed information on elemental and isotopic abundances (Engelmann et al. 1990; Wiedenbeck et al. 2001), including the peaked shape of the secondary-to-primary nuclei ratio (e.g., B/C, sub-Fe/Fe) and abundances of long-lived radionuclides (such as ^{10}Be , ^{26}Al , ^{36}Cl , and ^{54}Mn). These measurements are used to derive the (model-dependent) diffusion coefficient and the size of the Galactic volume filled with CRs (Strong & Moskalenko

1998; Ptuskin & Soutoul 1998; Webber & Soutoul 1998), the so-called halo. Models of CR propagation are in reasonable agreement with available data (e.g., Strong et al. 2007; Trotta et al. 2011), with a few exceptions including the unexpected rise in the positron fraction observed by PAMELA (Adriani et al. 2009).

The data recently collected by three experiments, ATIC-2 (Wefel et al. 2008; Panov et al. 2009), CREAM (Ahn et al. 2010; Yoon et al. 2011), and PAMELA (Adriani et al. 2011), indicate a break (hardening) of the spectra of the most abundant CR species above a rigidity of a few hundred GV. The break rigidity, ρ_{br} , is best measured by PAMELA and occurs at approximately the same rigidity for p and He, $\rho_{\text{br}} = 240$ GV. The PAMELA data for $10 \text{ GV} \lesssim \rho < \rho_{\text{br}}$ agree very well with the earlier data from AMS and BESS (see Alcaraz et al. 2000; Haino et al. 2004 and Figure 1 of Adriani et al. 2011), while ATIC-2 data points for $\rho < \rho_{\text{br}}$ are somewhat lower. We take the PAMELA data as the most accurate for $\rho < \rho_{\text{br}}$. For $\rho > \rho_{\text{br}}$, ATIC-2 results agree well with those of CREAM. The change in the spectral index (below/above the break) is estimated as $\Delta_{\text{br}} = \gamma(> \rho_{\text{br}}) - \gamma(< \rho_{\text{br}}) = 0.15$, and is the same for protons and He.

Another important feature of the CR spectra discovered by these experiments is the difference between the spectral indices of CR protons and He. This has been speculated for a long time (e.g., Biermann et al. 1995, and references therein), but the experimental uncertainties were too large to be conclusive (see the collection of CR proton and He measurements in Moskalenko et al. 2002). The new measurements by the ATIC-2, CREAM, and PAMELA experiments confirm this with high significance. The spectrum of He is found to be harder than the spectrum of protons for energies below at least 10^4 GeV per nucleon. The difference between the proton and He spectral indices calculated by Adriani et al. (2011) using the PAMELA data is $\Delta\gamma = 0.10$, and it is approximately the same above and below ρ_{br} . Within the statistical and systematic uncertainty, the measured p/He flux ratio appears to be a smooth function of rigidity, continuous at ρ_{br} . This shows that the difference in the spectral slope of protons and He nuclei persists into the ultra-relativistic regime.

There is also fine structure in the spectra that may provide some clues to the nature of the observed features: PAMELA

¹ W. W. Hansen Experimental Physics Laboratory Stanford University, Stanford, CA 94305, USA

² Kavli Institute for Particle Astrophysics and Cosmology, Stanford University, Stanford, CA 94305, USA

³ Science Institute, University of Iceland, Dunhaga 5, IS-107 Reykjavik, Iceland

data clearly show a spectral softening at the break rigidity (which we refer to as the “dip”, below). Adriani et al. (2011) have shown the softening to be statistically significant at the 95% confidence level for the spectra as functions of particle rigidity, and the 99.7% level for the same data in terms of kinetic energy per nucleon. The softening is more pronounced in the He spectrum.

Rather than proposing a detailed interpretation of the observed features, in this paper we discuss broad categories of models, hereafter called *Scenarios*, and propose their observational tests. A particular realization of each scenario is called *Calculation*. The quantitative analysis is done using the GALPROP code⁴ (Strong & Moskalenko 1998).

2. SCENARIOS

2.1. Reference case

Scenario R: Reference scenario. First, we introduce a reference CR propagation model based on the pre-PAMELA data. In this scenario, the CR injection spectrum above 10 GV is a single power law up to the “knee” in the CR spectrum, with the same spectral index for all CR species. The rigidity dependence of the diffusion coefficient is also taken as a single power-law for all energies. The CR source distribution is described in Section 3. *Scenario R* provides reasonable agreement with the pre-PAMELA data, but it cannot reproduce the spectral features evident in the new data discussed in this paper: the difference between proton and He spectra, the spectral break, or the dip. Below, we describe several broad categories of models that encompass viable explanations for these new features. Comparing predictions for these other models for quantities other than CR proton and He spectra with predictions of *Calculation R* qualitatively illustrate the significance of the difference between different scenarios.

2.2. p/He ratio

The confirmation of a significant difference between proton and He spectral indices poses a challenge for theories of CR acceleration and propagation. Whatever the physical cause of this difference in spectra may be, it seems to affect heavier nuclei in the same way as it does He (see, e.g., Ahn et al. 2009, for spectra of nuclei), giving them a harder spectrum than that of protons.

Diffusive shock acceleration indeed predicts the spectrum of He to be harder than that of protons due to its lower Z/A ratio, but only for non-relativistic energies (e.g., Ellison et al. 1997). A p/He ratio declining with energy at ultra-relativistic energies could be produced by shocks expanding in a non-uniform medium. This would be the case if particle acceleration by the shocks is rapid, and the He abundance (Ohira & Ioka 2011) or magnetic field orientation (Biermann et al. 1995) varies in a way that enhances He acceleration in young shocks. Alternatively, propagation effects could be responsible for the p/He spectral difference. The second order Fermi process (reacceleration) in the interstellar medium makes the He spectrum harder due to its lower Z/A ratio, but this does not extend to the ultra-relativistic regime (e.g., Strong et al. 2007).

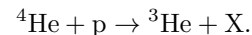
Blasi & Amato (2011a) suggested that spallation of CR nuclei ($Z > 1$) may lead to hardening of their spectra. This is because the lower energy CRs have longer confinement times in the Galaxy, so the hardening occurs for rigidities where

the spallation timescale is short compared to the CR diffusive escape timescale. Our calculations include spallation of all nuclei species, the default with GALPROP. However, as our results for *Calculation R* show (see Section 4), the effect of spallation on the He spectrum is insignificant, and the p/He ratio above 10 GV is flat. Still, in order to investigate this hypothesis, we introduce *Scenario S*. With this scenario, we demonstrate that, with some model tuning, fragmentation may indeed lead to hardening of the He spectrum. We also assess the consequences of the required model modifications.

Scenario S: Spallation effects. The fraction of fragmented CR nuclear species depends on their total inelastic cross section and the effective grammage encountered by the CR species in the Galaxy. Inelastic cross section fits used in Blasi & Amato (2011a), taken from Hörandel et al. (2007), are somewhat larger than those used in our calculations (Barashenkov 1993; Barashenkov & Polyanski 1994). Besides, the gas number density used in calculations by Blasi & Amato (2011a) yields a significantly larger grammage than in our standard models. To segregate these effects, we consider two scenarios $S_{1,2}$. Calculations representing both scenarios adapt the cross section fits from Hörandel et al. (2007). In *Scenario S₂*, we additionally increased the gas number density relative to *Scenario R* by a factor of 2. Note that these calculations use the GALPROP code, which was adapted to incorporate the above-mentioned inelastic cross sections, whereas the production of fragments (daughter isotopes) is calculated using a standard set of cross sections and remains unchanged.

Our calculations show that the required hardening of the He ($^3He + ^4He$) spectrum can be achieved only if we assume a considerable increase in grammage and simultaneously adopt a set of total inelastic cross sections from Hörandel et al. (2007), *Calculation S₂*. However, this leads to an overproduction of secondary species in CRs, such as antiprotons and boron, so that the calculated B/C ratio does not agree with the data. With our standard gas distribution based on astronomical data (Moskalenko et al. 2002), *Calculation S₁*, the amount of hardening is insufficient to provide agreement with the PAMELA p/He ratio. The p/He ratios obtained in *Calculations S₁* and *S₂* are shown in the top panel of Figure 1. The calculated B/C ratio and \bar{p} flux are shown in the middle and bottom panels, respectively. Read on and see Figures 2 and 3 for details on the parameters of *Calculation R* also shown in Figure 1.

Another important point to consider here is that the measurements of PAMELA, ATIC-2 and CREAM are not sensitive to the isotopic composition of CR fluxes. The He fluxes reported by these experiments and used throughout this paper are, in fact, the sum of 3He and 4He species. The dominant channel of 4He spallation is the reaction



This reaction leads to a hardening of the interstellar 4He spectrum because lower energy nuclei experience more spallation events. However, due to production of 3He in the same reaction, the *total* He spectrum does not harden as much as 4He alone. Further spallation of secondary 3He , as well as fragmentation of 4He into products other than 3He , eventually lead to the total He spectrum hardening. Still, the effect of spallation on the total He spectrum is not as strong as on 4He alone. Equation (2.1) in Blasi & Amato (2011a) indicates that 3He was not included in their calculations. Therefore, their

⁴ The project web site <http://galprop.stanford.edu/>

results would be relevant only for the $p/{}^4\text{He}$ ratio.

This is illustrated in Figure 1, where we also plot the ratio of $p/{}^4\text{He}$ in *Calculation S₂* for reference. It can be seen that the overall shape of the $p/{}^4\text{He}$ ratio matches the measured p/He ratio well, however, a significant fraction of secondary ${}^3\text{He}$ changes the shape so that the calculated p/He ratio can not be adjusted to match the data simultaneously at all rigidities (1 GV – 10 TV).

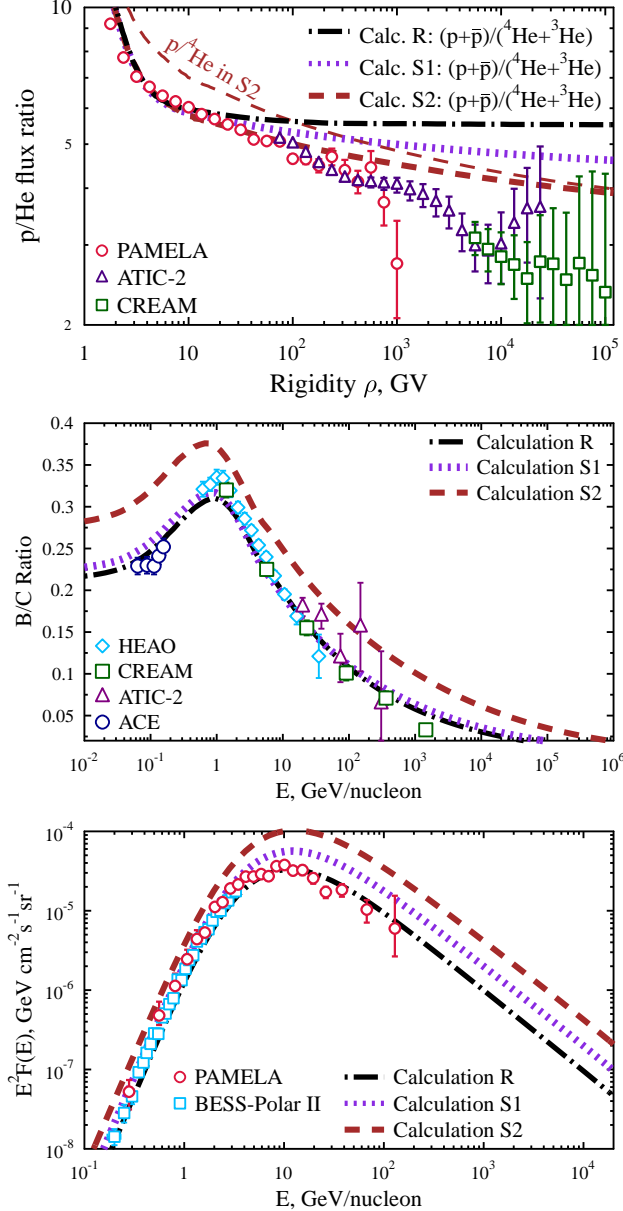


Figure 1. (color in online version) CR proton to He, B/C ratio and antiproton flux (sources of data as in Figures 5, 7, 8), together with calculation results. *Calculation S1* and *Calculation S2* use the same spallation cross sections and z_H/D ratio as those of Blasi & Amato (2011a). In *Calculation S2*, the gas density is increased by a factor of 2 with respect to *Calculation S1*. Results of *Calculation S1* are consistent with the B/C ratio data, but slightly overpredict \bar{p} measurements. However, note that the effect of spallation is not sufficient to make the slope of the p/He ratio agree with the PAMELA data. In *Calculation S2*, spallation is stronger due to increased grammage, and the p/He ratio is reproduced better, but the B/C ratio and \bar{p} flux are overpredicted.

Our conclusion is that the adjustments of propagation model required to reproduce the observed p/He ratio in *Scenario S₂* conflict with the production of secondary CR species. Therefore, in the rest of this work we use the standard propagation parameters, cross section fits, and gas distribution (same as in *Calculation R*). To reproduce the p/He ratio we use an *ad hoc* modification for the CR injection spectra. That is, in our calculations, we assume that nuclei heavier than H are injected into the ISM with a harder spectrum than protons. The difference between the spectral indices of protons and heavier nuclei is the same for all rigidities and is $\Delta_{p/\text{He}} = 0.07$. Figure 5 shows the p/He ratio resulting from this modification (see below for parameters of other calculations shown in this figure). The figure shows that the data reported by PAMELA, ATIC-2, and CREAM can be reproduced by this model.

2.3. Spectral break and dip

We consider the following scenarios for an explanation of the break at ρ_{br} and the dip just below ρ_{br} : (i) interstellar propagation effects, (ii) modification of CR injection spectrum at the sources, (iii) composite Galactic CR spectrum, (iv) effects of local sources at low energies ($\rho < \rho_{\text{br}}$), and (v) effects of local sources at high energies ($\rho > \rho_{\text{br}}$). Particular realizations of these scenarios (calculations) are discussed in detail in Section 3.2; their parameters are summarized in Table 1.

Scenario P: interstellar Propagation effects. Transport of CRs in the ISM is a subject to considerable uncertainties, because the properties of interstellar magnetic turbulence are not very well known (Elmegreen & Scalo 2004; Scalo & Elmegreen 2004). This makes CR observations a valuable indirect probe of quantitative features of particle transport (e.g., the diffusion coefficient, D) in the Galaxy. Therefore, in this scenario, the break in the observed proton and He spectra is attributed to a change in CR transport properties at rigidity ρ_{br} . This scenario is represented by *Calculation P*, which has a break in the rigidity dependence of the diffusion coefficient at $\rho = \rho_{\text{br}}$. For $\rho < \rho_{\text{br}}$, we use the functional form of $D(\rho)$ obtained in the earlier comprehensive analysis of CR data by Trotta et al. (2011), and for $\rho > \rho_{\text{br}}$, we adjust the rigidity dependence of $D(\rho)$ to match the observations of PAMELA, ATIC-2, and CREAM, as discussed above.

Scenario I (a): CR Injection effects, source with a spectral break interpretation. Existing models of CR production by SNR shocks (e.g., Caprioli et al. 2010; Ptuskin et al. 2010) predict a smooth spectrum of CR particles injected by a SNR into the Galaxy. Such models usually consider a shock in the semi-infinite medium or assume spherical symmetry. The spectrum predicted by these models may gradually harden with energy between 10 GeV and 100 TeV, but not as rapidly as in the PAMELA data. Note that particle transport, magnetic turbulence generation, and nonlinear feedback of particles and magnetic fields on shock structure are not strictly constrained in these models. The spectrum of particles leaking from a SNR shock has never been observed directly. It is therefore conceivable that with some parameter tuning, present models of particle acceleration may predict a more pronounced hardening in the spectrum of particles injected into the ISM, consistent with the new data. Alternatively, particle acceleration models that take into account the asymmetry of SNRs may predict a break in the particle spectrum produced by a single SNR. For example, in the model of Biermann et al.

(2010), the break, or upturn, occurs due to the contribution of the SNR's polar cap. This case, hereafter referred to as *Scenario I (a)*, is represented by *Calculation I*, which features a Galaxy-wide source spectrum with a hardening at ρ_{br} . The diffusion coefficient does not have a break in this scenario.

Scenario I (b): CR Injection effects, composite source interpretation. While SNRs (isolated or in superbubble regions) are believed to be the primary sources of Galactic CRs, different classes of supernovae and their environments, as well as other CR sources, can combine to produce the observed CR spectrum. Generally speaking, different types of CR sources could have different spatial distributions throughout the Galaxy. In this work, we make the simplifying assumption (i) that there are only two types of CR sources, and (ii) the spatial distributions are the same for both types of CR sources. If one source dominates the low energy part of the CR spectrum, and the other the high energy part, then *Calculation I*, with a hardening of the Galactic CR source at ρ_{br} , adequately encompasses this composite source scenario as well. We use the same computational setup to calculate the observed quantities for *Scenario I (a)* and *Scenario I (b)*, and we call it just *Calculation I*. A subtle advantage of the composite source interpretation of *Calculation I* (i.e., in *Scenario I (b)*) is its ability to explain the dip more naturally than the source with an inherent break scenario (see discussion of the dip in Section 4).

Scenario L: local Low energy source. This scenario encompasses interpretations that assume that the observed spectral break is caused by a local source dominating the CR spectrum at low rigidities, $\rho < \rho_{\text{br}}$. Unlike *Scenario I (b)*, the present scenario assumes that the low-energy source is not typical for the Galaxy as a whole. This scenario is formulated as *Calculation L*, in which the Galactic CR spectrum is hard, matching the observations of PAMELA, ATIC-2, and CREAM for $\rho > \rho_{\text{br}}$. For $\rho < \rho_{\text{br}}$, the flux of Galactic CRs is lower than the observed flux, and we assume that the difference is accounted for by the hypothetical local source. We assume the extreme case of a very local low energy source. This means that we do not calculate propagation of CRs from that source and only the Galactic sources with the hard spectrum are used to calculate the production of secondaries and the diffuse Galactic γ -ray emission. This scenario contrasts with *Scenario I (b)*, where the sources of low-energy CRs are distributed across the Galaxy. The case of intermediate local source extent falls in between *Scenario L* and *Scenario I (b)*.

Scenario H: local High energy source. This scenario is analogous to *Scenario L*, but with Galactic sources dominating the CR flux for $\rho < \rho_{\text{br}}$, and the spectral break produced by a local high-energy source dominating the observed flux for $\rho > \rho_{\text{br}}$. The calculation representing this scenario is referred to as *Calculation H*. The assumption of the high-energy source being very local is made in this calculation identically to how it was done in *Calculation L*, i.e., the production of secondaries and the diffuse Galactic γ -ray emission is determined solely by the Galactic CR sources.

3. CALCULATIONS

3.1. GALPROP code

The GALPROP project began in late 1996 (Strong & Moskalenko 1998) and has been in continuous development since. The code is available from the dedicated website where a facility for users to run the

code via online forms in a web browser⁵ is also provided (Vladimirov et al. 2011).

The GALPROP code solves the CR transport equation for a given source distribution and boundary conditions for all CR species. This includes diffusion, a galactic wind (convection), diffusive reacceleration in the ISM, energy losses, nuclear fragmentation, radioactive decay, and production of secondary particles and isotopes:

$$\frac{\partial \psi}{\partial t} = q(\mathbf{r}, p) + \nabla \cdot (D_{xx} \nabla \psi - \mathbf{V} \psi) + \frac{\partial}{\partial p} p^2 D_{pp} \frac{\partial}{\partial p} \frac{1}{p^2} \psi - \frac{\partial}{\partial p} \left[\dot{p} \psi - \frac{p}{3} (\nabla \cdot \mathbf{V}) \psi \right] - \frac{1}{\tau_f} \psi - \frac{1}{\tau_r} \psi, \quad (1)$$

where $\psi = \psi(\mathbf{r}, p, t)$ is the density per unit total particle momentum, $\psi(p) dp = 4\pi p^2 f(p) dp$ in terms of phase-space density $f(p)$, $q(\mathbf{r}, p)$ is the source term, D_{xx} is the spatial diffusion coefficient, \mathbf{V} is the convection velocity, reacceleration is described as diffusion in momentum space with diffusion coefficient D_{pp} , $\dot{p} \equiv dp/dt$ is the momentum loss rate, τ_f is the time scale for fragmentation, and τ_r is the time scale for radioactive decay. The numerical solution of the transport equation is based on a Crank-Nicholson (Press et al. 1992) implicit second-order scheme. The spatial boundary conditions assume free particle escape, e.g., $\psi(R_h, z, p) = \psi(R, \pm z_h, p) = 0$, where R_h and z_h are the boundaries for a cylindrically symmetric geometry.

If reacceleration is included, D_{pp} is related to D_{xx} (Berezinskii et al. 1990; Seo & Ptuskin 1994):

$$D_{pp} D_{xx} = \frac{4p^2 v_{\text{Alf}}^2}{3\delta(4 - \delta^2)(4 - \delta)w}, \quad (2)$$

where w characterizes the level of turbulence (we take $w = 1$ because only the quantity v_{Alf}^2/w is relevant), and $\delta = 1/3$ for a Kolmogorov spectrum of interstellar turbulence or $\delta = 1/2$ for a Kraichnan cascade (but can also be arbitrary).

The source function q is

$$q(\mathbf{r}, \rho) = q_{\text{pri}}(\mathbf{r}, \rho) + \sum q_{\text{sec}}(\mathbf{r}, \rho), \quad (3)$$

where q_{pri} represents the primary CR sources, and the q_{sec} term is for the sources of secondary isotopes (i.e., nuclear reactions in the ISM), and $\rho \equiv pc/Ze$ is the magnetic rigidity where p is momentum and Ze is the charge. The distribution of primary Galactic CR sources used in this work is based on the supernova distribution from Case & Bhattacharya (1998).

In this work, the steady-state solutions of Equation (1) are obtained assuming the source functions are time-independent and integrating the equation over a long enough time interval. The accelerated solution technique is used, where the initial time step, $\Delta t = 10^9$ yr, is large compared to the propagation time scale, and after $N_s = 20$ iterations, Δt is reduced by a factor of 2, etc., until Δt becomes small compared to the shortest time scale in the system (in our case, 10 yr, to accommodate the rapid energy losses of leptons).

The details of physical processes and data used in the GALPROP code, as well as the numerical scheme, can be found elsewhere. A complete list of relevant publications is available in Vladimirov et al. (2011); the aforementioned GALPROP web site contains additional information and publications.

⁵ <http://galprop.stanford.edu/webrun/>

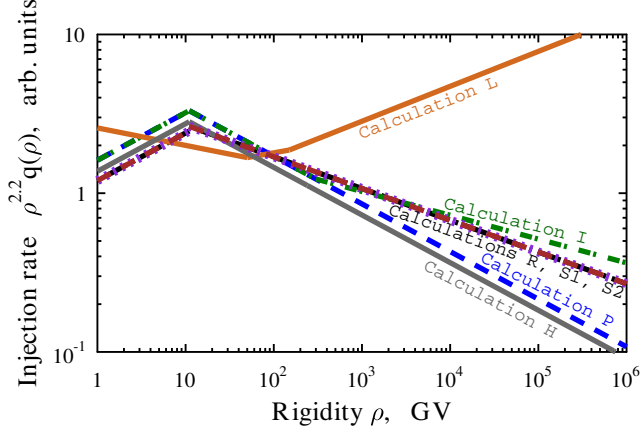


Figure 2. (color in online version) Galactic CR source injection spectrum for Calculations *R*, *S*, *P*, *I*, *L*, and *H* in arbitrary units. The normalization for the injection spectrum was chosen to match local measurements of proton and He spectra. For all calculations, the lines represent the Galactic CR source injection spectrum. “Local” sources, present in *Calculation L* and *Calculation H*, are not shown here. The “local” source fluxes at Earth in *Calculation L* and *Calculation H* were obtained as the difference between the observed and propagated Galactic fluxes.

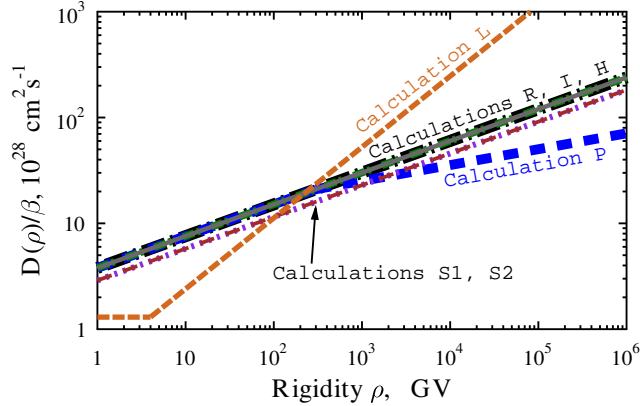


Figure 3. (color in online version) Diffusion coefficient of CRs in the Galaxy defined by Equation (4). The values of the D coincide for Calculations *R*, *I*, *L* and *H*. For *Calculation S*, the value of D is slightly smaller at all energies. For *Calculation P*, a break in the diffusion coefficient is assumed, changing $\delta_1/\delta_2 = 0.30/0.15$ at $\rho_0 = 300$ GV.

3.2. Calculation Setups

The parameters of our calculations are summarized in Table 1. Figures 2 and 3 show the diffusion coefficients and the injection spectra used for the different scenarios.

Calculation R is the reference case for this study. We choose the diffusive-reacceleration model, which has been used in a number of studies utilizing the GALPROP code (e.g., Moskalenko et al. 2002; Strong et al. 2004; Ptuskin et al. 2006b; Abdo et al. 2009, and references therein). In this and other calculations the spatial diffusion coefficient is given by

$$D_{xx} = \beta D_0 \left(\frac{\rho}{\rho_0} \right)^\delta \quad (4)$$

where D_0 is the normalization at rigidity ρ_0 and $\beta \equiv v/c$. The power-law index $\delta = 1/3$ corresponds to Kolmogorov diffusion (see Section 3.1). For *Calculation R*, we use $\delta = 0.30$, and a normalization for the diffusion coefficient $D_0 = 2.4 \times 10^{29} \text{ cm}^2 \text{ s}^{-1}$ with $\rho_0 = 300$ GV, which is consistent with the best-fit values obtained by Trotta et al. (2011) from a Bayesian analysis of a diffusive-reacceleration model using the GALPROP code.

In this work, we assume the primary CR source function is a broken power law in particle rigidity:

$$q_{\text{pri}}(\mathbf{r}, \rho) \propto Q(\mathbf{r}) \left(\frac{\rho}{\rho_{\text{inj}1}} \right)^g, \quad (5)$$

$$g = \begin{cases} g_1 & \text{for } \rho < \rho_{\text{inj}1} \\ g_2 & \text{for } \rho_{\text{inj}1} \leq \rho < \rho_{\text{inj}2} \\ g_3 & \text{for } \rho \geq \rho_{\text{inj}2} \end{cases}$$

For a given choice of injection spectrum a break at a few GV ($\rho_{\text{inj}1}$) is required in diffusive-reacceleration models to agree with the observed CR spectra at low energies. It is also possible to specify a second spectral break for $q_{\text{pri}}(\mathbf{r}, \rho)$ at higher rigidities $\rho_{\text{inj}2} \approx \rho_{\text{br}}$. This is done in *Calculation I*, described below. For *Calculation R*, we chose $g_1 = -1.9$, $g_2 = g_3 = -2.4$ (i.e., no break at $\rho_{\text{inj}2}$) and $\rho_{\text{inj}1} = 11$ GV for all nucleons, which is consistent with the findings of Trotta et al. (2011). The electron injection spectrum in all calculations is similar to that from Ackermann et al. (2010), with spectral index in rigidity $\Gamma = 1.60/2.50$ below/above a break rigidity of 4 GV, and a second steepening to $\Gamma = 5.0$ above 2 TV.

Matching the B/C ratio below 1 GeV in diffusive reacceleration models is known to require large values of v_{Alf} . We chose $v_{\text{Alf}} = 32 \text{ km s}^{-1}$, the halo size $z_h = 4$ kpc, and the normalization of the propagated CR proton spectrum was tuned to the observed flux $N_p = 10.7 \times 10^{-12} \text{ cm}^{-2} \text{ s}^{-1} \text{ sr}^{-1} \text{ MeV}^{-1}$ for $\rho = 10^3$ GV. These values were obtained by slightly adjusting the best-fit values obtained by Trotta et al. (2011) to achieve a good agreement with the PAMELA proton spectrum for $\rho < \rho_{\text{inj}1}$. These adjusted values are still within one mean square deviation of the posterior mean found by Trotta et al. (2011). In all figures, black lines represent the input and output quantities pertaining to *Calculation R*.

Calculation P has the same parameters as the reference *Calculation R* except: (i) the injection spectrum of protons above $\rho_{\text{inj}1}$ has a softer power-law index to give agreement with the PAMELA data below ρ_{br} ; (ii) the injection spectra of He and heavier elements ($A > 1$) have a power-law index harder than that of protons by $\Delta_{p/\text{He}}$ for all rigidities; (iii) the rigidity dependence of the diffusion coefficient, Equation (4), has a break at rigidity ρ_0 (i.e., $\delta_1 \neq \delta_2$). The break in the rigidity dependence of the diffusion coefficient is introduced to match the observed break in the CR spectrum. Besides, we choose $\rho_0 \approx \rho_{\text{br}}$ so that ρ_0 is slightly larger than ρ_{br} for better agreement with the data for $\rho > \rho_{\text{br}}$. The normalization of the proton flux has been adjusted in *Calculation P*, along with the abundance of He, to agree with PAMELA data at all energies (the abundances of heavier nuclei were changed by the same factor as He). The results for *Calculation P* are shown with blue lines in all figures.

Calculation I differs from *Calculation R* in the following ways: (i) the index of the proton injection spectrum is softer than in *Calculation R* for $\rho_{\text{inj}1} < \rho < \rho_{\text{inj}2}$; (ii) the injection spectrum has two breaks, i.e., $g_2 \neq g_3$, and (iii) nuclei are

Table 1
Summary of model parameters

Parameter	Description	Calculations					
		<i>R</i>	<i>S</i> ₁ (<i>S</i> ₂)	<i>P</i>	<i>I</i>	<i>L</i>	<i>H</i>
INJECTION							
<i>g</i> ₁ (protons)	Injection index for $\rho < \rho_{\text{inj}1}$	-1.90	-1.90	-1.90	-1.90	-2.31	-1.90
$\rho_{\text{inj}1}$	First break in CR injection spectrum, GV	11	11	11	11	50	11
<i>g</i> ₂ (protons)	Injection index for $\rho_{\text{inj}1} < \rho < \rho_{\text{inj}2}$	-2.40	-2.40	-2.50	-2.50	-2.10	-2.50
$\rho_{\text{inj}2}$	Second break in CR injection spectrum, GV	300	150	...
<i>g</i> ₃ (protons)	Injection index for $\rho_{\text{inj}2} < \rho$	-2.35	-1.98	...
$\Delta_{p/\text{He}}$	For nuclei, $g_i(A > 1) = g_i(\text{protons}) + \Delta_{p/\text{He}}$	0.07	0.07	0.07	0.07
<i>N</i> _{<i>p</i>}	Flux of protons at $\rho = 10^3$ GV, in units $10^{-12} \text{ cm}^{-2} \text{ sr}^{-1} \text{ s}^{-1} \text{ MeV}^{-1}$	10.7	10.7	8.56	8.56	8.50	7.28
<i>n</i> (H)/ <i>n</i> ₀ (H)	Multiplication factor for the gas number density relative to standard gas maps	...	1.0 (2.0)
⁴ He/ ¹ H	Abundance of ⁴ He relative to ¹ H in CR sources at 10^3 GeV/nucleon. Abundances of other isotopes are proportional to ⁴ He.	0.0685	^{0.0870} (0.1075)	0.0840	0.0935	0.0980	0.0826
PROPAGATION							
<i>v</i> _{Alf}	Alfvén speed	32	25	32	32	...	32
<i>D</i> ₀	Diffusion coefficient at ρ_0 , in units $10^{28} \text{ cm}^2 \text{ s}^{-1}$	21	16	21	21	1.3	21
δ_1	δ in Equation (4) for $\rho < \rho_0$	0.30	0.30	0.30	0.30	0.00	0.30
ρ_0	Diffusion coefficient reference rigidity, GV	300	300	300	300	4.0	300
δ_2	δ for $\rho > \rho_0$	0.15	...	0.67	...

injected with a harder spectrum than protons, similar to *Calculation P*. This calculation produces a CR spectrum at Earth with a break at ρ_{br} closely matching that of *Calculation P*, but due to a different physical assumption. Namely, it is the spectral break in the CR injection spectrum that produces the break in *Calculation I*, whereas in *Calculation P*, it occurs because of a break in the diffusion coefficient. The results of this calculation are shown as green lines.

Calculation H combines two components. One component is produced by the Galactic CR sources and propagated using GALPROP with the same parameters as *Calculation I*. This component does not have a break in the CR injection spectrum at $\rho_{\text{inj}2}$ and its normalization was tuned to match the proton and He spectra for $\rho < \rho_{\text{inj}2}$. Another component is produced by a hypothetical local source, which contributes to the total flux only for $\rho > \rho_{\text{br}}$. We do not calculate CR propagation for the local source; instead, we calculate its spectrum at Earth by subtracting the Galactic source spectrum from the data of ATIC-2 and CREAM for $\rho > \rho_{\text{br}}$. As discussed in Section 4, this represents the assumption that the local source is nearby and not very powerful. To compute secondary particles and isotopic ratios in this calculation, we assume that isotopic abundances in the local and Galactic sources are similar, and that the local source supplies no secondary particles at Earth. This lowers, for instance, the B/C ratio and antiprotons for $\rho > \rho_{\text{br}}$. The diffuse γ -ray emission from the Galaxy is calculated using only CR fluxes from the Galactic source. Gray lines represent this calculation in plots.

Calculation L features a local source that contributes to the low-energy part of the CR spectrum ($\rho < \rho_{\text{br}}$). The local source is included in the same way as in *Calculation H*, i.e., its propagated spectrum is calculated as the difference between the observed CR spectrum and the propagated Galactic component. As in *Calculation H*, we do not calculate the propagation of CRs from the local source, and assume that its flux contains no secondary species. However, this calculation is

very different from all others, because the *low energy* CRs are a mix of particles which have undergone Galactic propagation and recently accelerated particles from the local source. Because of that, the propagation parameters for this calculation should be estimated simultaneously with the parameters of the local source, as in Moskalenko et al. (2003).

Assuming that CRs from the local source are produced so recently that they contain no secondary nuclei, one can calculate the B/C ratio for *Scenario L* in the energy range where the local source contribution is non-negligible. Matching the B/C ratio in the diffusive-reacceleration model is quite challenging (see below), so we have chosen a plain diffusion model for this case, which required significant modifications of all other parameters. Most importantly, to maintain the agreement with B/C at high *and* low energies, the diffusion coefficient has a stronger rigidity dependence for $\rho > \rho_0 = 4$ GV with $\delta_2 = 2/3$, and a flatter rigidity dependence for $\rho < \rho_0$. The injection spectrum was adjusted accordingly to agree with the PAMELA proton spectrum and the B/C measurements below 1 GeV per nucleon. For *Calculation L*, lines in all plots are orange.

To illustrate the rationale for our choice of propagation parameters for *Calculation L*, we also introduce *Calculation L**, which has the same parameters as in *Calculation R*, except $g_2 = g_3 = 2.35$, and $\Delta_{p/\text{He}} = 0.07$. The local source spectrum is determined by subtracting the spectrum of propagated particles from the Galactic sources from the observed spectrum of CR species, as in *Scenario L*. *Calculation L** is only illustrated in Figure 7 with light yellow lines.

The results of *Calculation L* and *Calculation L** are shown in Figure 7. Because the local source does not produce boron, the B/C ratio in the range 1–10 GeV per nucleon is too low (*Calculation L**). Matching the B/C data requires a larger GCR confinement time, which, in turn, requires a lower value of the diffusion coefficient at these energies (or a larger halo size). Correspondingly, to maintain good agreement with the

data above 10 GeV per nucleon, the CR confinement time at these energies cannot be increased too much, which requires a larger value of δ_2 . With a larger confinement time below 10 GeV per nucleon, the diffusive reacceleration becomes too strong resulting in too many energetic protons around 1 GeV, and thus v_{Alf} should be reduced. In fact, we found that in this scenario the best agreement with the PAMELA data for protons is achieved with $v_{\text{Alf}} = 0$ (i.e., no reacceleration) and $\delta_1=0$ below a few GV. This is because any finite v_{Alf} hardens the proton spectrum below 1 GeV too much to match the PAMELA data. Because the B/C ratio below 1 GeV per nucleon is reduced by the local source contribution, matching the ACE data requires that the flux of the local source to be relatively small. This dictates the choice of the concave Galactic source spectrum, i.e., $g_1 > g_2 > g_3$ (see Table 1), which is similar to the theoretical predictions by Ptuskin et al. (2010), and explains the choice of parameters for *Calculation L*.

Note that *Calculation L** cannot be considered physical because it does not reproduce the B/C data. It is included only as an illustration. To understand the implications of a local CR source producing the observed spectral break in the proton and He spectra one should only use the results of *Calculation L*.

Finally, in *Calculation S₁* all parameters are the same as in *Calculation R*, except for the diffusion coefficient D_0 and the Alfvén speed v_{Alf} . D_0 is reduced by approximately 25%, which makes the ratio z_H/D_0 equal to that in the calculations of Blasi & Amato (2011a). v_{Alf} is reduced accordingly to avoid a large bump in the proton spectrum at low energies. In addition, the propagation calculations use a different set of total inelastic cross sections (equations [6]–[8] in Hörandel et al. 2007). *Calculation S₂* has the same parameters as *Calculation S₁*, but the density of all gas components in the Galactic disk (i.e., H I, H II and H₂) is multiplied by 2. The results of *Calculation S_{1,2}* are compared with *Calculation R* in Figure 1.

4. RESULTS

The results of *Calculations R, S, P, I, L, and H*, as specified in Table 1, are summarized in Figure 1 (discussed above) and Figures 4 through 10. Figures 4 and 5 show the proton and He spectra and their ratio. Figure 1, illustrating *Scenario S*, is discussed in detail in Section 2.2 and in the figure caption. We do not discuss the origin of the difference between the slopes of the proton and He spectra in Section 4 (e.g., the effect of spallation on CR spectra), instead concentrating on scenarios explaining the spectral break. *Calculations P, I, L and H* were designed to reproduce the observed proton and He spectrum and, therefore, cannot be used to constrain any of these scenarios. However, their predictions for CR anisotropy and the production of secondary species (B/C ratio, \bar{p} flux and \bar{p}/p ratio) differ and are shown in Figures 6, 7, 8, and 9. Predictions for the diffuse Galactic γ -ray emission at intermediate latitudes ($10^\circ < |b| < 20^\circ$) are compared with the data collected by the *Fermi*-LAT in Figure 10.

4.1. Proton and He spectra

Proton and He spectra calculated for the different scenarios and their ratio are plotted in Figures 4, 5. The bins in rigidity for protons are different from the bins for He in all experiments. Because of this, the experimental data points of PAMELA, ATIC-2 and CREAM shown in Figure 5 were obtained by interpolating the proton and He spectra, along with

their errors, and by calculating the p/He ratio on a grid. For simplicity, solar modulation for all spectra is taken into account using the force-field approximation (Gleeson & Axford 1968) with a modulation potential $\Phi = 450$ MV.

While the reference case, *Calculation R*, provides satisfactory agreement with pre-PAMELA data by construction, it naturally misses all newly discovered features: an overall harder He spectrum, the spectral break at ρ_{br} , along with the dip just below ρ_{br} . The difference between the spectrum of He and protons at all energies was phenomenologically included in all other calculations except *Calculation R*, which is reflected in the considerably better agreement with the p/He ratio data in Figure 5.

Calculation P: A break in the rigidity dependence of the diffusion coefficient leads to a corresponding break in the CR spectrum at Earth. In order to match the data, we assumed the change in the value of δ (see Equation [4]) from $\delta_1 = 0.30$ to $\delta_2 = 0.15$ at $\rho_0 \approx \rho_{\text{br}}$. Two corresponding physical quantities can be derived from these values. Assuming that the change in δ is caused by a difference between the properties of interstellar MHD turbulence on scales smaller and larger than a certain length scale Λ_{br} , we can estimate this length to be of order of the gyroradius of 300 GV particles. The gyroradius of a particle of rigidity ρ in magnetic field B is

$$r_g = 4 \times 10^{-2} \left(\frac{\rho}{1 \text{ GV}} \right) \left(\frac{B}{5 \mu\text{G}} \right)^{-1} \text{ AU}. \quad (6)$$

For a characteristic interstellar magnetic field of order of a few μG , this implies a change in turbulence properties on length scales of the order of $\Lambda_{\text{br}} \approx 10$ AU. If the quasilinear theory of turbulent particle diffusion applies to CR transport in the ISM, the value $\delta_2 = 0.15$ corresponds to turbulence spectral index, $\alpha = -2 + \delta_2 = -1.85$, which is harder than a Kolmogorov spectrum, $\alpha = -5/3$. Note that the direction in which the index α changes across the transition wavenumber $k = \Lambda_{\text{br}}^{-1}$ is opposite to the transition of the turbulent cascade from the inertial to dissipative regime. In our case, the turbulence spectrum hardens, rather than softens, above $k = \Lambda_{\text{br}}^{-1}$.

Calculation I assumes a change of the power-law index of CR injection spectrum at $\rho_{\text{inj}2} = 300$ GV, which produces a break at $\rho_{\text{br}} \approx \rho_{\text{inj}2}$ in the CR spectrum at Earth. The dip is not produced in this calculation.

Calculation L (dashed orange lines in Figure 4 and 5) agrees with the p/He ratio and spectral break, and also reproduces the dip just below ρ_{br} . This is possible because of the combination of the hard spectrum from Galactic sources that matches the data for $\rho > \rho_{\text{br}}$ (solid orange lines in Figure 4) with a local low-energy source having a sharp turnover just below ρ_{br} (dotted orange lines in Figure 4). Note that despite reproducing the proton and He spectra and resembling other calculations, *Calculation L* has a very different set of propagation parameters. It does not include reacceleration, has a diffusion coefficient with a break from $\delta_1 = 0$ to $\delta_2 = 0.67$ at $\rho_0 = 4$ GV, and assumes a concave Galactic source spectrum. These parameters are chosen to provide good agreement with the observed B/C ratio over the wide energy range spanned by the data.

In *Calculation H*, the spectral break at ρ_{br} is produced by the local source beginning to dominate the CR spectrum above ρ_{br} . We assume that the Galactic source has the same power-law index for $\rho > \rho_{\text{br}}$ as the low-energy CR spectrum.

The observed continuity of the p/He ratio and its slope at

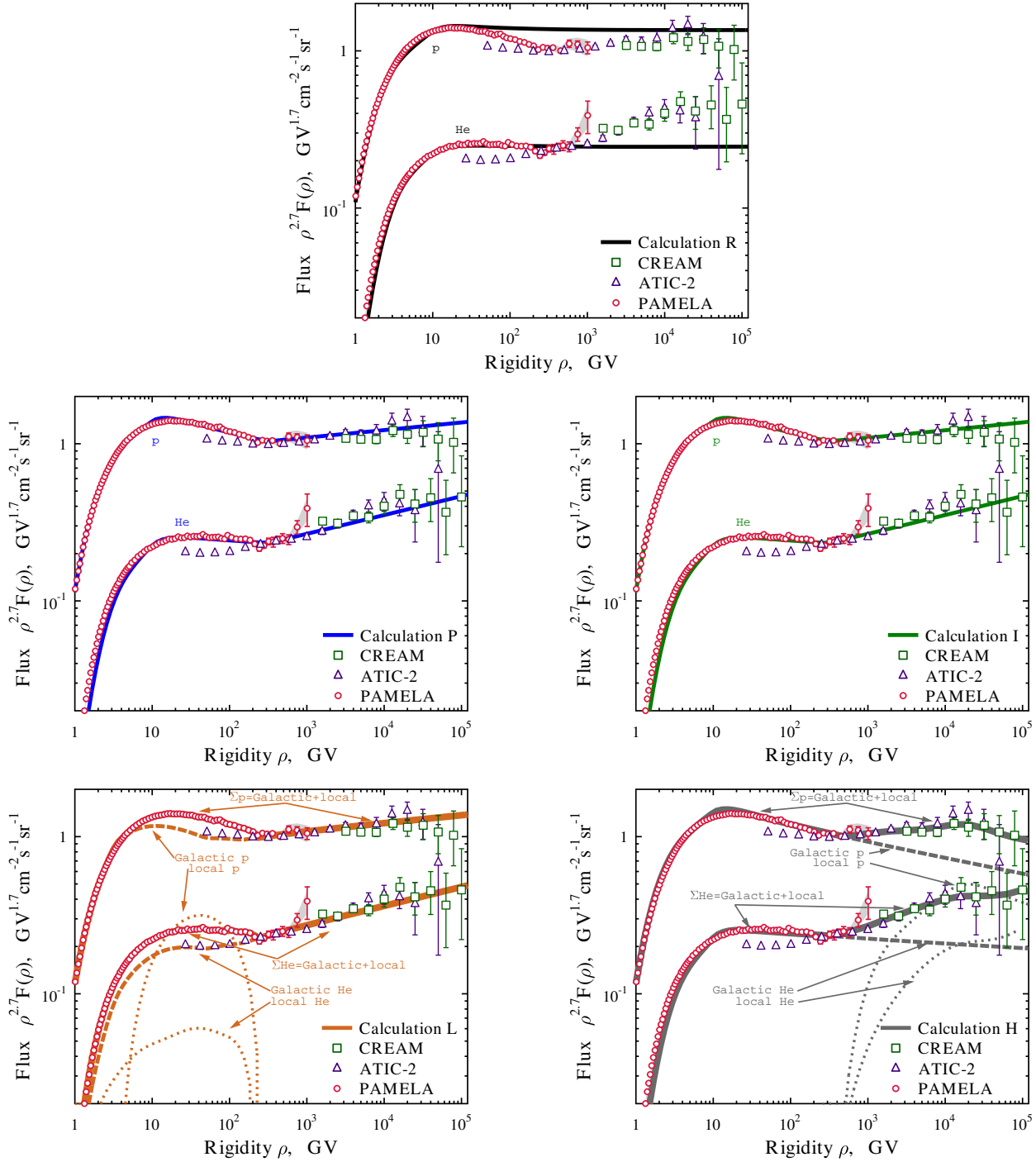


Figure 4. (color in online version) CR proton and He spectra: data of PAMELA (Adriani et al. 2011), ATIC-2 (Wefel et al. 2008; Panov et al. 2009), and CREAM (Ahn et al. 2010; Yoon et al. 2011) together with calculation results. For *Calculations L* and *H*, dashed lines show the net CR flux comprised of the Galactic source contribution (solid lines) and a “local” source contribution (dotted lines). “Local” source spectra were obtained by subtracting the Galactic source fluxes from an interpolation of data (the CR propagation calculation was not done for the “local” source component). Solar modulation in all spectra is taken into account using force-field approximation with a modulation potential $\Phi = 450$ MV. See discussion in Section 4.1.

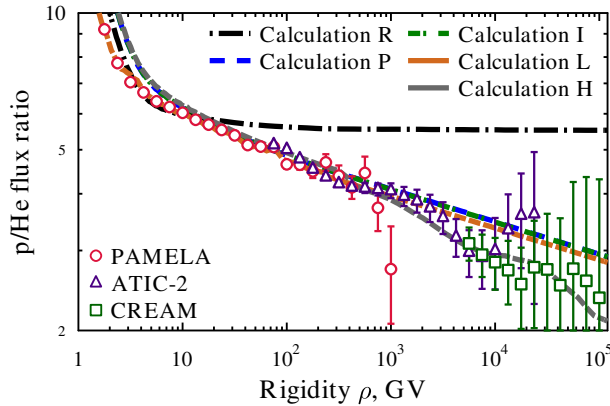


Figure 5. (color in online version) CR proton to He flux ratio: data of PAMELA (Adriani et al. 2011), ATIC-2 (Wefel et al. 2008; Panov et al. 2009), and CREAM (Ahn et al. 2010; Yoon et al. 2011), together with calculation results. The p/He points for experimental data were obtained by interpolating the measured fluxes of protons and He along with respective errors and calculating the p/He ratio on a grid. See discussion in Section 4.1.

ρ_{br} within statistical and systematic uncertainties is very important. In *Scenario P*, this property of the p/He ratio comes about naturally. Indeed, if the injection spectrum is continuous, then protons and He nuclei experience the change in diffusion coefficient in the same way, and the p/He ratio is unaffected. However, matching this observation in the framework of a composite source spectrum (*Scenario L*, *Scenario H* or *Scenario I (b)*) requires an additional assumption of the H to He ratio to be the same at the sources producing the low-energy and high-energy particles.

For the analysis of all calculations discussed above, the dip in the spectrum, if it is significant, may lead to important implications. One possible explanation for the dip may be provided in the framework of *Scenario L* and *Scenario I (b)*. It can naturally appear if the spectrum of the low-energy CR sources (Galactic or local) turns sharply over just below ρ_{br} , rather than continuing as a power law up to the knee in the CR spectrum. Indeed, it is trivial to prove that for any two power-law spectra, their sum always hardens with energy. Thus, for the softening below ρ_{br} to occur, the low-energy source spectrum may not be a pure power law; the sharpness of the dip suggests that it must steeply turn over below ρ_{br} , where the dip occurs. The dip may also be explained in the framework of *Scenario P*, if a corresponding dip in the spectrum of MHD turbulence responsible for CR confinement in the Galaxy is assumed. It is not possible to explain the dip with *Scenario H*, because the low-energy source is assumed to have a power-law spectral shape extending all the way to the knee.

4.2. Anisotropy

For all scenarios, we calculated the anisotropy of the high-energy CR flux at the location of the Sun due to diffusive escape of CRs from the Galaxy. The results are presented in Figure 6, along with data. References to individual experiments may be found in Ptuskin et al. (2006a); see also Strong et al. (2007) for a color version of the plot. The anisotropy, dominated by the radial component, is highly sensitive to the choice of the diffusion coefficient and the spatial distribution of CR sources. Our calculation ignores the effect of nearby CR sources, which may be significant (Ptuskin et al. 2006a;

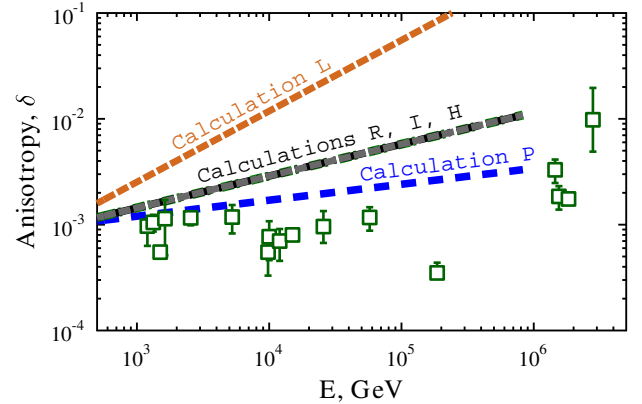


Figure 6. (color in online version) CR flux anisotropy: data from Ptuskin et al. (2006a), together with calculation results. The anisotropy was calculated as the ratio of diffusive flux in the radial direction to the isotropic flux at the corresponding energy. *Calculations R, S, I, L* and *H* all predict the same value of anisotropy, and their respective lines overlap. The result of *Calculation P* is different due to a different form of the CR diffusion coefficient. See discussion in Section 4.2

Blasi & Amato 2011b), but is not very well defined and depends on the assumed distances to the sources and their ages. However, if the diffusive component of the anisotropy dominates in a certain energy range, two conclusions may be drawn from this plot. The first one is that *Scenario P* can be distinguished from the others with improved CR proton anisotropy data. The second point illustrated by our calculation is that the diffusion regime of *Calculation P* with $D \propto \rho^\delta$ and $\delta = 0.15$ agrees with the available data better than $\delta = 0.30$. *Calculation L*, due to a harder dependence of the diffusion coefficient on rigidity, predicts a higher degree of anisotropy, which disagrees with the data more than the other calculations. However, this may be not conclusive given that the choice of the propagation model in this scenario is quite arbitrary. In case of *Calculation H*, the plotted line corresponds to only the Galactic source, while the direction and magnitude of the local source flux anisotropy above ρ_{br} is unknown.

4.3. Boron to carbon ratio

The B/C ratio for all scenarios discussed in the paper is shown in Figure 7. Predictions of *Calculation R* and *Calculation I* coincide at all energies, while *Calculation P* predicts a larger B/C ratio for $\rho > \rho_{\text{br}}$, which is a consequence of the smaller diffusion coefficient in *Calculation P*. In the case of *Calculation L* and *Calculation H*, the results include the effect of the local CR source. CR boron is produced by fragmentation of heavier elements and decay of ^{10}Be . If the local source is very nearby, its flux should contain no boron. But, the abundance of (primary) carbon should be close to the interstellar value, which results in a lower B/C ratio in the net flux than without the local source.

To find the the B/C ratio for *Calculation H* and *Calculation L*, we assume that the local source produces no boron, and assume the flux of local source carbon to be proportional to that of He, with the same carbon and He abundance as in the Galactic source. *Calculation H* predicts a lower B/C for $\rho > \rho_{\text{br}}$, because the local high-energy source supplies primary carbon, but not secondary boron at these energies. *Calculation L*, in which the parameters were tuned to provide

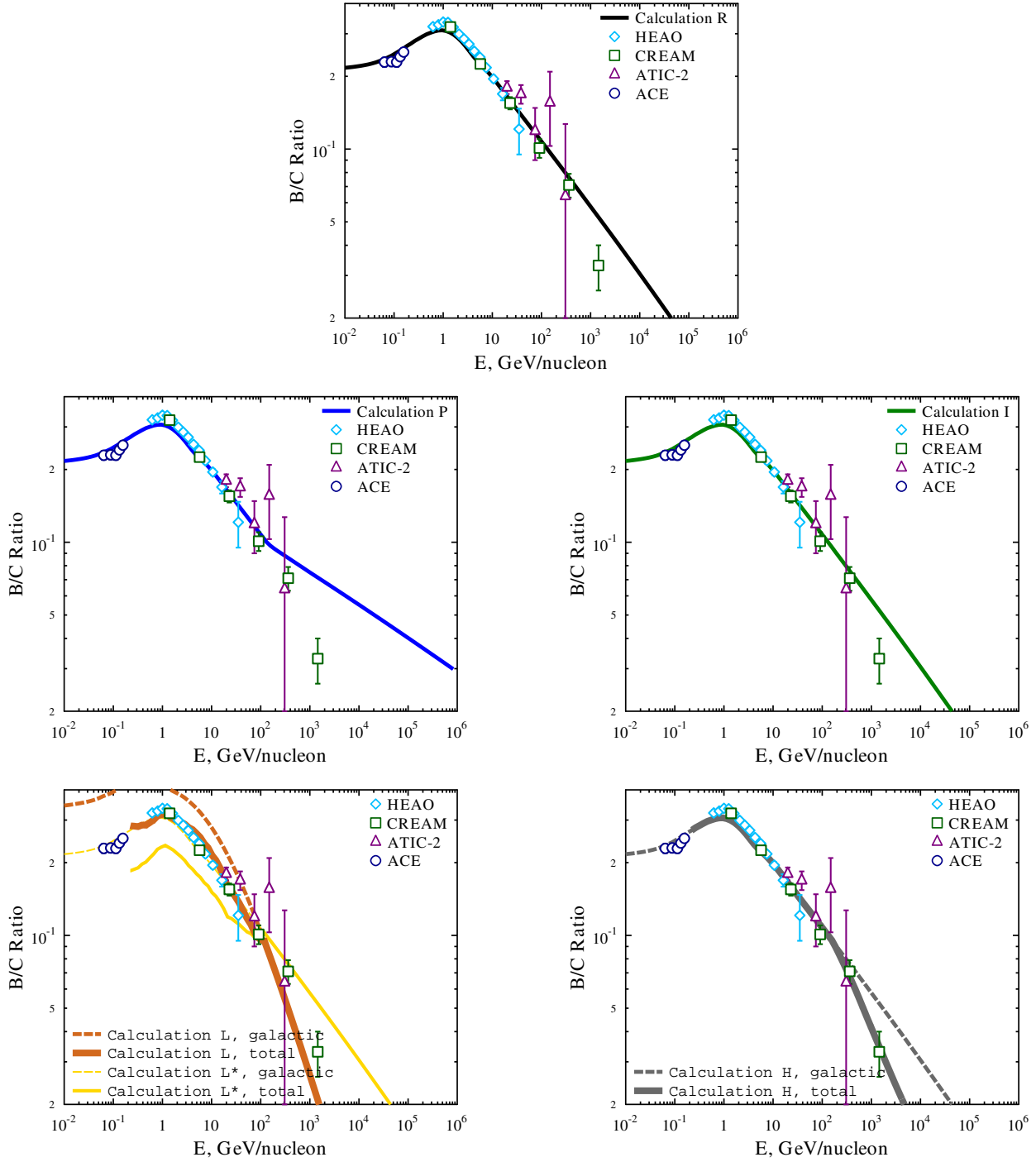


Figure 7. (color in online version) CR boron-to-carbon flux ratio. Data: Davis et al. (2000) (ACE), Engelmann et al. (1990) (HEAO-3), Ahn et al. (2008) (CREAM), and Panov et al. (2008) (ATIC-2). Predictions of *Calculation R* and *Calculation I* coincide at all energies. The prediction of *Calculation P* is larger above ρ_{br} due to a break in the rigidity dependence of the diffusion coefficient. For *Calculation L* and *Calculation H*, dashed lines show the ratio of just the Galactic source, while solid lines show the B/C ratio including the contribution of the “local” source component. *Calculation L* was designed to match the B/C ratio at all energies. It is consistent with the high-energy data, but predicts a lower B/C at high energies due to a harder slope for the diffusion coefficient. The yellow lines (*Calculation L**) illustrate B/C obtained if the parameters of *Calculation L* were identical to those of *Calculation I*, but without a break in the injection spectrum, including the “local” source contribution. Additional discussion in Section 4.3

good agreement with the B/C measurements at all energies, differs from all other calculations above 100 GeV per nucleon due to the harder rigidity dependence of the diffusion coefficient.

Experimental data at low energies (below 1 GeV per nucleon) were collected by ACE (Davis et al. 2000), and for high energies by HEAO-3 (Engelmann et al. 1990), CREAM (Ahn et al. 2008) and ATIC-2 (Panov et al. 2008). The uncertainties in the data are still too large to rule out any of the scenarios considered in this paper, but data collected by future experiments, such as AMS-2 may be more constraining.

4.4. Antiproton flux and \bar{p}/p ratio

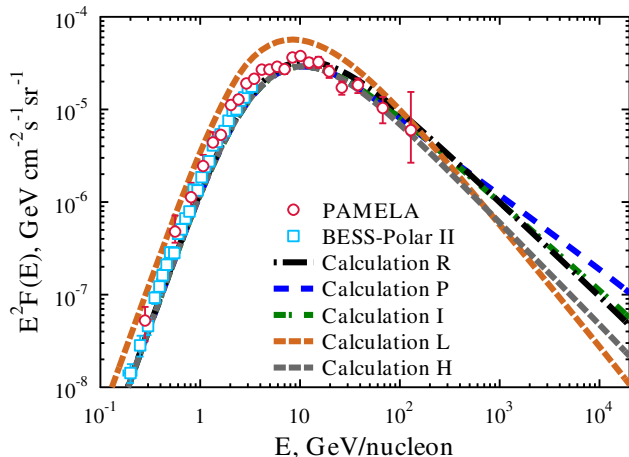


Figure 8. (color in online version) CR antiprotons: data from Adriani et al. (2010) and Abe et al. (2011) together with calculation results. See discussion in Section 4.4

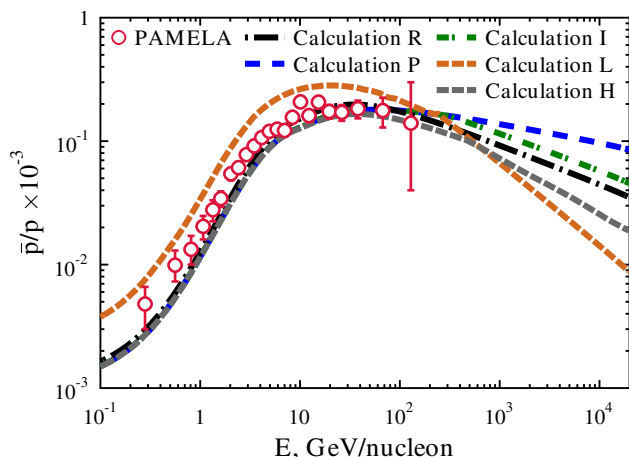


Figure 9. (color in online version) CR antiproton to proton ratio: data from Adriani et al. (2010) together with calculation results. See discussion in Section 4.4

The antiproton flux, another probe of CR propagation, is plotted in Figure 8, and \bar{p}/p ratio in Figure 9, together with the PAMELA data from Adriani et al. (2010) and the

BESS-Polar II data from Abe et al. (2011). *Calculations R, P, I, and H* are in good agreement with data below 100 GeV. Differences between all calculations are apparent above ~ 1 TeV, but no data are currently available.

Calculation L, due to a larger particle confinement time, predicts a factor of ~ 2 excess of \bar{p} below 100 GeV. In *Calculations L* and *H*, the local source was assumed to be completely devoid of primary or secondary antiprotons. More accurate data covering a larger energy range may help eliminate some of the scenarios, and the AMS-2 mission may provide these data.

4.5. Diffuse γ -ray emission

Predictions of the γ -ray emission at intermediate Galactic latitudes ($10^\circ < |b| < 20^\circ$) are plotted in Figure 10 along with the data reported by Abdo et al. (2010, see the online supplementary material). Following Abdo et al. (2010), the flux of the inverse Compton (IC) component was increased by a factor of 2 to obtain a good fit to the data. Our calculations include γ -ray emission produced by hadronic and leptonic components of CRs (i.e., π^0 -decay, IC, and bremsstrahlung channels), as well as point sources, and the isotropic extragalactic emission. The relative differences in the *total* γ -ray flux between the considered scenarios are quite small and are considerably smaller than if only the π^0 -decay channel is considered (as in Donato & Serpico 2011).

Predictions of all calculations, except *Calculation L*, agree with the published *Fermi*-LAT data, within the uncertainty band. *Calculation L* predicts a slightly lower γ -ray emission below 10 GeV. Note that even the reference *Calculation R*, which does not agree with the PAMELA data, satisfactorily reproduces the γ -ray data.

For all scenarios we calculated the γ -ray spectrum up to 1 TeV, but the *Fermi*-LAT team has not published on the data above 100 GeV so far. At these energies, the softer spectrum of protons (above ρ_{br}) from Galactic sources in *Calculation H* produces less pions resulting in a smaller flux of pionic γ -rays compared to other scenarios. However, the contributions of comparable IC component and isotropic emission in the range 100 GeV – 1 TeV are not affected by the proton spectrum. Therefore, even at these energies the difference between the *total* γ -ray emission in *Calculation H* and other calculations is significantly smaller than the difference in the π^0 -decay channel alone. Unsurprisingly, *Calculation P* cannot be distinguished from *Calculation I* using the γ -ray data alone, because calculations for both scenarios result in nearly the same spectrum of CR protons, even though it is achieved via different mechanisms.

As the *Fermi* mission continues, the statistical uncertainty will be reduced as data accumulates, and systematic errors are likely to be brought down by improved data analysis. It should be noted, however, that the analysis of the diffuse γ -ray emission is complicated by many factors, including the uncertainty in the spatial distribution for the CR sources and the loosely constrained spectrum of CR electrons over the Galaxy responsible for inverse Compton emission that dominates high-energy γ -rays.

5. DISCUSSION

In this paper, we used the diffusive-reacceleration model to describe the CR transport. Alternatively, we could have employed a plain diffusion model, where the diffusive reacceleration is inefficient ($v_{AIf} = 0$), the diffusion coefficient is constant below a break rigidity ~ 10 GV, along with a stronger

Table 2
Do the scenarios agree with CR observations?

Observation	<i>Scenario R/S</i>	<i>Scenario P</i>	<i>Scenario I (a)</i>	<i>Scenario I (b)</i>	<i>Scenario L</i>	<i>Scenario H</i>
The break (hardening of p and He spectra at ρ_{br}), Figure 4	No	Yes, due to a break in the diffusion coefficient	Yes, due to a break in the injection spectrum	Yes, due to the assumption of a composite source	Yes, due to the assumption of a local low energy source	Yes, due to the assumption of a local high energy source
The ‘dip’ (softening of CR spectra at $\rho < \rho_{\text{br}}$), Figure 4	No	No, unless the diffusion coefficient has a corresponding ‘dip’	No	No, but the ‘dip’ can be explained by assuming that the low-energy Galactic source turns over below ρ_{br} .	Yes	No
Difference between p and He spectra, see Figures 4 and 5	Yes, if parameters are tuned to increase grammage and cross sections, as in <i>Scenario S</i> .	Yes, phenomenologically introduced	Yes, phenomenologically introduced	Yes, phenomenologically introduced	Yes, phenomenologically introduced	Yes, phenomenologically introduced
Continuity of p/He ratio at ρ_{br} , Figure 5	Yes, but does not match the value of p/He ratio	Yes, no additional assumptions	Yes, no additional assumptions	Yes, but only if the different source classes inject with the same p/He ratio at ρ_{br}	Yes, but only if the local and Galactic sources classes inject with the same p/He ratio at ρ_{br}	Yes, but only if the local and Galactic sources classes inject with the same p/He ratio at ρ_{br}
CR anisotropy due to diffusive escape of CRs above 1 TeV, Figure 6	Overpredicts	Overpredicts, but less than other scenarios	Overpredicts	Overpredicts, but the possibility of different spatial distributions of the two source classes must be considered	Overpredicts	Overpredicts; the local source, if it extends above 1 TeV, may affect anisotropy
B/C ratio above 1 GeV/nuc, Figure 7	Yes	Yes, but differs from other scenarios above ρ_{br} ; possible discrimination with more accurate data	Yes	Yes	Yes, by design	Yes
\bar{p} flux (PAMELA), Figure 8	Yes, above a few GeV	Yes, but differs from other scenarios above ρ_{br}	Yes, above a few GeV	Yes, above a few GeV	No	Yes, above a few GeV
γ -ray observations by <i>Fermi</i> -LAT, Figure 10	Yes	Yes	Yes	Yes	No	Yes

dependence for higher rigidities ($\delta \sim 2/3$). Using this kind of model would have the following effect on our calculations.

The proton and He spectra can be reproduced with appropriate adjustments of the source spectra injection indices together with the rigidity dependence of the diffusion coefficient. However, only for the diffusive-reacceleration model (with some adjustments, see Section 2.2) is it naturally possible to reproduce the rigidity dependence of the p/He ratio. For *Scenario S* (and that considered by Blasi & Amato 2011a), the escape time at low energies is too short in the plain diffusion model to provide the required hardening, and hence to reproduce the observed p/He ratio.

The CR anisotropy measurements seem to favor *Scenario P* with its weak rigidity dependence for the diffusion coefficient. But, the hard-to-estimate effect(s) of local CR sources may change this conclusion. The diffusive-reacceleration model predicts anisotropy which is a factor of a few higher than the data. For the case of distributed Galactic sources, the stronger rigidity dependence of diffusion required in a plain diffusion model would give a predicted anisotropy even higher than the diffusive-reacceleration model, by orders of magnitude above

~ 10 TeV.

The B/C ratio can be reproduced with a plain diffusion model, even at low energies with the introduction of ad hoc breaks in the diffusion coefficient. For the rigidity dependence of the diffusion coefficient, the high energy data are consistent for either model due to the large error bars.

The \bar{p} flux and \bar{p}/p ratio at high energies calculated in the plain diffusion model would be steeper than the diffusive-reacceleration model because of the strong rigidity dependence for diffusion coefficient in the former. For either *Scenario I (a)* or *Scenario I (b)* for the case of the plain diffusion model they could be obtained by shifting the predictions for *Scenario L* down by a factor ~ 2 (see the discussion in Ptuskin et al. 2006b), which would then be consistent with the PAMELA \bar{p} measurements within the error bars. However, at higher energies it would give a steeper spectrum for the \bar{p} flux.

Unfortunately, the diffuse γ -ray emission cannot be used to distinguish between the diffusive-reacceleration and plain diffusion models because the ambient CR spectra are tuned to the same local measurements.

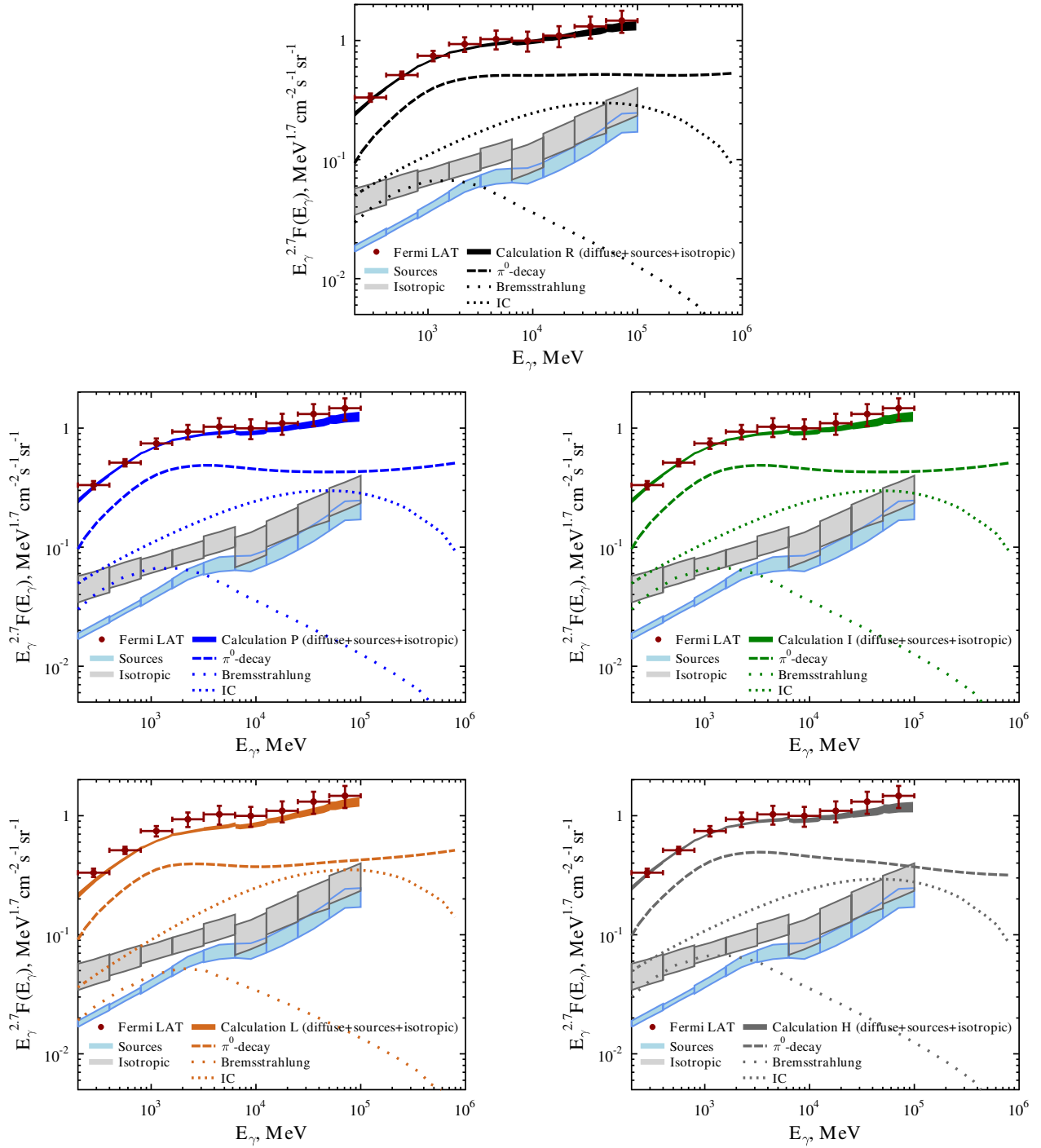


Figure 10. (color in online version) Diffuse γ -ray emission from intermediate Galactic latitudes: data from Abdo et al. (2010) together with calculation results. The data are the diffuse γ -ray intensities averaged over all Galactic longitudes and intermediate Galactic latitudes $10^\circ < |b| < 20^\circ$, as reported by Abdo et al. (2010) (available in the online supplementary material to the article). See discussion in Section 4.5

6. SUMMARY

We have presented scenarios reproducing the spectral features in CR proton and He spectra (the p/He ratio dependence on energy, the dip, and spectral break) observed by ATIC-2, CREAM, and PAMELA. For each scenario, we performed CR propagation calculations in the framework of diffusive-reacceleration model (except *Scenario L*), using the GALPROP code. Differences between scenarios are reflected in the CR anisotropy and fluxes of secondary CR species: the B/C ratio at high energies, the antiproton flux and antiproton to proton ratio, as well as the diffuse Galactic γ -ray emission. Table 2 summarizes our results. We find the following:

(a) He spallation (*Scenario S*) may be involved in making the spectrum of He and heavier nuclei harder than protons. However, a significantly increased grammage traversed by CRs in the Galaxy is required to explain the p/He observations with spallation. This makes it problematic to match stable secondary CR isotope observations (B/C and antiprotons).

(b) Experimental uncertainty in the data on high energy B/C ratio does not allow us to rigorously reject any of the scenarios for the origin of the spectral break. However, more accurate measurements of high-energy B/C, expected from planned CR experiments, may be used for model rejection.

(c) Antiproton flux and \bar{p}/p ratio seem to disfavor the local source hypothesis (*Scenario L*). Measurements of \bar{p} and/or \bar{p}/p above 1 TeV may help differentiate between the other scenarios.

(d) Radial component of diffusive anisotropy of CR flux is too high in all scenarios, but the discrepancy is larger in *Scenario L*, while *Scenario P* predicts the lowest anisotropy. Local sources may significantly affect the CR anisotropy, and therefore our simple analysis applies only to energy range unaffected by local sources.

(e) Finally, the γ -ray data is in agreement, within the uncertainty range, with all scenarios, including *Scenario R*, even though the reference scenario does not agree with the new measurements for the CR proton and He spectra. *Scenario L* slightly underpredicts the γ -ray flux below a few GeV.

Most specific physical models explaining the p/He ratio, spectral break and the dip fall into one of the scenarios studied in this paper, or their combination. Data from experiments such as the *Fermi*-LAT and AMS-2 can be used to distinguish between some of these scenarios.

A. V. and I. V. M. acknowledge support from NASA Grant No. NNX09AC15G. T. A. P. acknowledges support from NASA Grant No. NNX10AE78G. The authors are grateful to P. Blasi, E. Orlando, and A. Strong for fruitful discussions and to P. Picozza and M. Boezio for sharing and discussing preliminary PAMELA results.

REFERENCES

Abbasi, R., et al. 2005, *Physics Letters B*, 619, 271
 Abbasi, R. U., et al. 2009, *Astroparticle Physics*, 32, 53
 Abdo, A. A., et al. 2009, *Physical Review Letters*, 103, 251101

—. 2010, *Physical Review Letters*, 104, 101101
 Abe, K., et al. 2011, ArXiv: 1107.6000
 Abraham, J., et al. 2010, *Physics Letters B*, 685, 239
 Ackermann, M., et al. 2010, *Phys. Rev. D*, 82, 092004
 Adriani, O., et al. 2009, *Nature*, 458, 607
 —. 2010, *Physical Review Letters*, 105, 121101
 —. 2011, *Science*, 332, 69
 Ahn, H. S., et al. 2008, *Astroparticle Physics*, 30, 133
 —. 2009, *ApJ*, 707, 593
 —. 2010, *ApJ*, 714, L89
 Alcaraz, J., et al. 2000, *Physics Letters B*, 490, 27
 Barashenkov, V. S. 1993, *Cross Sections of Interactions of Particles and Nuclei with Nuclei*, IINR, Dubna, Russia, p. 346, in Russian
 Barashenkov, V. S., & Polyanski, A. 1994, CROSEC code, Joint Institute for Nuclear Research, JINR E2-94-417
 Berezinskii, V. S., Bulanov, S. V., Dogiel, V. A., & Ptuskin, V. S. 1990, *Astrophysics of cosmic rays*, ed. Amsterdam: North-Holland, 1990, edited by Ginzburg, V. L.
 Biermann, P. L., Becker, J. K., Dreyer, J., Meli, A., Seo, E.-S., & Stanev, T. 2010, *ApJ*, 725, 184
 Biermann, P. L., Gaisser, T. K., & Stanev, T. 1995, *Phys. Rev. D*, 51, 3450
 Biskamp, D. 2003, *Magnetohydrodynamic Turbulence*, ed. Biskamp, D.
 Blasi, P., & Amato, E. 2011a, ArXiv: 1105.4521
 —. 2011b, ArXiv: 1105.4529
 Caprioli, D., Amato, E., & Blasi, P. 2010, *Astroparticle Physics*, 33, 160
 Case, G. L., & Bhattacharya, D. 1998, *ApJ*, 504, 761
 Davis, A. J., et al. 2000, in *American Institute of Physics Conference Series*, Vol. 528, *Acceleration and Transport of Energetic Particles Observed in the Heliosphere*, ed. R. A. Mewaldt, J. R. Jokipii, M. A. Lee, E. Möbius, & T. H. Zurbuchen, 421–424
 Donato, F., & Serpico, P. D. 2011, *Phys. Rev. D*, 83, 023014
 Drury, L. O., et al. 2001, *Space Sci. Rev.*, 99, 329
 Ellison, D. C., Drury, L. O., & Meyer, J. 1997, *ApJ*, 487, 197
 Elmegreen, B. G., & Scalo, J. 2004, *ARA&A*, 42, 211
 Engelmann, J. J., Ferrando, P., Soutoul, A., Goret, P., & Juliusson, E. 1990, *A&A*, 233, 96
 Gleeson, L. J., & Axford, W. I. 1968, *ApJ*, 154, 1011
 Haino, S., et al. 2004, *Physics Letters B*, 594, 35
 Haungs, A., Rebel, H., & Roth, M. 2003, *Reports on Progress in Physics*, 66, 1145
 Hörandel, J. R., Kalmykov, N. N., & Timokhin, A. V. 2007, *Astroparticle Physics*, 27, 119
 Kulikov, G. V., & Khristiansen, G. B. 1958, *Soviet Physics JETP*, 35, 635
 Moskalenko, I. V., Strong, A. W., Mashnik, S. G., & Ormes, J. F. 2003, *ApJ*, 586, 1050
 Moskalenko, I. V., Strong, A. W., Ormes, J. F., & Potgieter, M. S. 2002, *ApJ*, 565, 280
 Ohira, Y., & Ioka, K. 2011, *ApJ*, 729, L13+
 Panov, A. D., et al. 2008, in *International Cosmic Ray Conference*, Vol. 2, 3–6
 Panov, A. D., et al. 2009, *Bulletin of the Russian Academy of Science, Phys.*, 73, 564
 Press, W. H., Teukolsky, S. A., Vetterling, W. T., & Flannery, B. P. 1992, *Numerical recipes in FORTRAN. The art of scientific computing*
 Ptuskin, V., Zirakashvili, V., & Seo, E. 2010, *ApJ*, 718, 31
 Ptuskin, V. S., Jones, F. C., Seo, E. S., & Sina, R. 2006a, *Advances in Space Research*, 37, 1909
 Ptuskin, V. S., Moskalenko, I. V., Jones, F. C., Strong, A. W., & Zirakashvili, V. N. 2006b, *ApJ*, 642, 902
 Ptuskin, V. S., & Soutoul, A. 1998, *A&A*, 337, 859
 Scalo, J., & Elmegreen, B. G. 2004, *ARA&A*, 42, 275
 Seo, E. S., & Ptuskin, V. S. 1994, *ApJ*, 431, 705
 Strong, A. W., & Moskalenko, I. V. 1998, *ApJ*, 509, 212
 Strong, A. W., Moskalenko, I. V., & Ptuskin, V. S. 2007, *Annual Review of Nuclear and Particle Science*, 57, 285
 Strong, A. W., Moskalenko, I. V., & Reimer, O. 2004, *ApJ*, 613, 962
 Swordy, S. P. 2001, *Space Sci. Rev.*, 99, 85
 Trotta, R., Jóhannesson, G., Moskalenko, I. V., Porter, T. A., Ruiz de Austri, R., & Strong, A. W. 2011, *ApJ*, 729, 106
 Vladimirov, A. E., Digel, S. W., Jóhannesson, G., Michelson, P. F., Moskalenko, I. V., Nolan, P. L., Orlando, E., Porter, T. A., & Strong, A. W. 2011, *Computer Physics Communications*, 182, 1156
 Webber, W. R., & Soutoul, A. 1998, *ApJ*, 506, 335
 Wefel, J. P., Adams, Jr., J. H., Ahn, H. S., & et al. 2008, in *International Cosmic Ray Conference*, Vol. 2, *International Cosmic Ray Conference*, 31–34
 Wiedenbeck, M. E., et al. 2001, *Space Sci. Rev.*, 99, 15
 Yoon, Y. S., et al. 2011, *The Astrophysical Journal*, 728, 122